Advances of Deep Learning Applications in Ground-Penetrating Radar: A Survey

Zheng Tong[a,*], Jie Gao[b], Dongdong Yuan[c]

[a] *Université de Technologie de Compiègne, CNRS, UMR 7253 Heudiasyc, Compiègne, 60203, France.*
[b] *East China Jiaotong University, School of Transportation and Logistics, Nanchang 330013, China*
[c] *Chang'an University, School of Highway, Xi'an 710064, China*

Abstract

Deep learning has achieved state-of-the-art performance on signal and image processing. Due to the remarkable success, it has been applied in more challenging tasks, such as ground-penetrating radar (GPR) testing in civil engineering. This paper reviews methods involving deep leaning and GPR for civil engineering inspection and provides a classification based on the data types that they exploit. Based on the results of a comparison study, we conclude that methods using A-scan data slightly surpass the models using B- and C-scan data, though C-scan data is maybe the most promising in the further thanks to its complete space information. Two current limitations of deep learning exploiting GPR are its dependence on big data and overconfident decision-making. Therefore, benchmark GPR data sets and cautious deep learning are required.

Keywords: ground-penetrating radar (GPR), nondestructive testing (NDT), deep learning, data processing, intelligent inspection for civil engineering
2010 MSC: 00-01, 99-00

1. Introduction

Recent advancements in nondestructive testing (NDT) have made safety inspection in civil engineering more effective and precise than ever. So far,

*Corresponding author
Email address: zheng.tong@hds.utc.fr (Zheng Tong)

there are many types of NDT devices for structural health monitoring (SHM), mainly including infrared thermography, ultrasonic testing, ground-penetrating radar (GPR), and industrial radiography. Compared with other techniques for SHM, GPR is considered as one of the most powerful because of its desirable reliability and effectiveness.

The increasing precision of GPR data encourages the research community to exploit this richer data for solving several SHM tasks, such as defect recognition, location, even 3D reconstruction. Figure 1 presents a generic pipeline for processing a group of GPR data. Structure Scan data contain thousands of signals and/or points. Thus, some preprocessing methods are applied to reduce noises and/or restructure data, such as Gaussian filter [1] and KD-trees [2]. Following, feature extractors (e.g., convolutional operator [3] and Sobel operator [4]) are adopted in order to identify features related to the inspection task. After acquiring related features, recognition, location, feature point regression, and segmentation are conducted using highly nonlinear mapping, such as neural networks [5] and support vector machines [6]. In addition, feature points and segmentation results provide the possibility of 3D buried object reconstruction, such as structural cracks. In summary, traditional GPR inspection depends on two factors: (1) precision of GPR devices; (2) effectiveness of feature extractors and nonlinear mapping algorithms. Precision of GPR devices has been improved remarkably with the development of measurement technologies [7]. However, errors from feature extractors and nonlinear mapping algorithms are still inevitable, owing to their shallow structures.

Until recently, the breakthrough from the work of Krizhevsky et al. [8] tremendously changed the landscape of the GPR detection in civil engineering. Deep learning (DL) models, especially deep neural networks, now dominate on almost defect detection tasks using GPR devices, leading many NDT groups to redesign their systems. Although the concept of neural network has been proposed for a long time, the evolution of general processor units and the availability of large datasets make the main contribution to its recent tremendous success [9, 10].

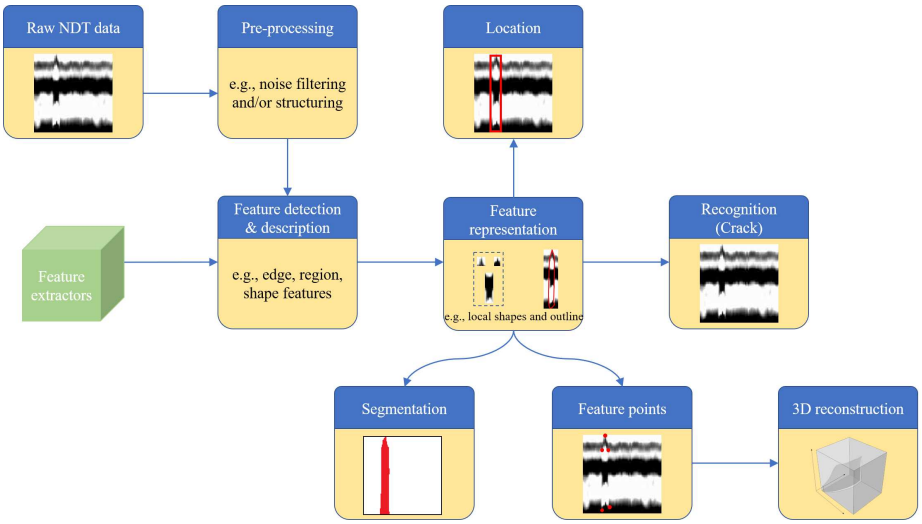

Figure 1: Generic pipeline for processing a group of GPR data.

In pace with the dominance establishment of DL in 1D and 2D data processing, it was soon adopted to combine with GPR techniques for SHM tasks. Motivated by this evolution, this paper surveys the main studies and presents an overview of existing DL models for civil engineering inspection tasks via GPR. Section 2 provides related works of GPR technologies in civil engineering to make the paper more self-contained, followed by a introduction to the conception of deep learning and the architectures used so far in the problems of GPR data processing in Section 3. Afterward, the advances of DL with GPR as the main body of this paper is presented in Section 4. Finally, conclusions are discussed in Section 5.

2. Ground-Penetrating Radar in Civil Engineering

In this section, we start from a brief recall of GPR principles and main configurations so far in civil engineering in Section 2.1. Further, we review the traditional methods for GPR data processing in Section 2.2, including signal-based processing (Section 2.2.1) ~~,~~ and image-based processing (Section 2.2.2)~~, and model-based processing (Section ??)~~. Finally, the current trends of GPR

data processing are discussed in Section 2.3.

2.1. GPR Principles and Main Configurations

GPR, as a geophysical inspection technique, transmits electromagnetic waves that can penetrate building structures. ~~A portion of the~~ The transmitted electromagnetic waves are reflected ~~when they hit a surface, whose electromagnetic properties are different from those of the mediums~~by subsurface boundaries at which there are electrical property contrasts. Then, the reflected waves are received by an antenna and used for SHM.~~structural health monitoring.The propagation of the electromagnetic waves is mainly effected by the dielectric properties of the mediums. Theoretically, the rules can be described by the Maxwell's equations as~~

$$\nabla \times \vec{E} = -\frac{\partial(\vec{B})}{\partial t},$$

$$\nabla \times \vec{H} = \vec{J} + \frac{\partial(\vec{D})}{\partial t},$$

$$\nabla \cdot \vec{D} = q,$$

$$\nabla \cdot \vec{B} = 0,$$

~~and the constitutive relationships as~~

$$\vec{J} = \sigma\vec{E},$$

$$\vec{D} = \varepsilon\vec{E},$$

$$\vec{B} = \mu\vec{H}.$$

~~Here, $\vec{E}$ is the strength vector of the electric field; $\vec{B}$ is the density vector of the magnetic flux; $\vec{H}$ is the intensity vector of the magnetic field; $\vec{J}$ is the density vector of the electric current; $\vec{D}$ is the electric displacement vector; q and t are the electric charge density and the time, respectively. Thus, the combination of Eq. ?? and Eq. ?? provides the possibility for the comprehensive interpretation of the received GPR waves in civil engineering.~~

There are mainly two types of GPRs used in the field of civil engineering based on their antenna configurations. ~~GPR systems that transmit impulses only with a specific frequency are~~ A GPR system that uses a short wavelength pulse signal with ultra-wide bandwidth in the frequency domain is called *pulsed radar*, while the one transmits impulses with individual frequencies is named *stepped frequency continuous-wave radar*. In general, the applications of GPR in civil engineering is mostly related to the use of *pulsed radar* because of its major easiness of usage and data interpretation. Furthermore, *pulsed radar* can be classified into two groups: ground-coupled and air-coupled. In the first group, the GPR antenna directly contacts with the ground, while the antenna kept a constant height with the surface in the second case.

The selection of antenna frequency, as another main configuration, can be considered as a compromise between the maximum detection depth and the expected object resolution. Expected object resolution means the minimum visible size of an object that a GPR can detect. Figure 2 provides a rough overview. Generally, higher frequencies can give a higher resolution but can penetrate a medium shallower than lower frequencies. In addition, the selection of the frequency range also should take the attenuation effects in various mediums into account.~~For example, an impulse with a specific frequency can easily penetrate dense wet clays but propagate in dense wet clays with difficulty.~~

2.2. Data Processing Techniques in GPR

From the first utilization of GPR in tunnel investigation in the 1970s [11], the GPR applications have extended to the assessment of damage conditions [12, 13], the evaluation of structure thickness [14], the detection of buried objects and defects [15, 16], the analysis of soil characteristics [17, 18], even novel perspectives of the possible to characterize mechanical properties of structures and materials based on their reflected electromagnetic waves [19, 20]. Data processing techniques are the key of the GPR data interpretation for these applications. The traditional techniques can be classified into ~~three~~ two parts: signal-based methods ~~,~~ and image-based methods~~, and model-based methods~~.

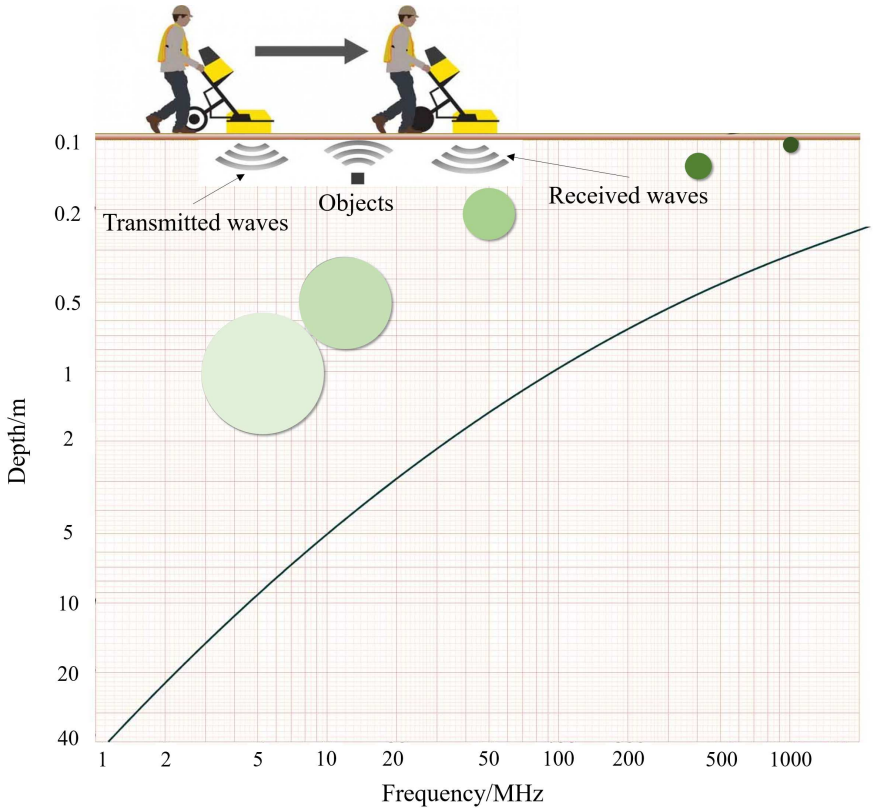

Figure 2: A compromise between penetrations depth and the target resolution for a frequency range.

In this section, we present a ~~discussion of the three~~ recall of the two parts.

2.2.1. Signal-based processing

In the signal-based methods, researchers focus on reducing the effects of background noise and interference phenomenon owing to inhomogeneous mediums. The processed data are used to interpret A-scan data. The signal-based methods can be classified into band-passing filtering [21, 22], time-varying gain [23, 24], and resolution improvement [25, 26].

However, these methods with promising performance always require desirable knowledge of both electromagnetic waves and SHM. It leads these methods cannot be widely used in SHM. For example, Li et al. [27] utilized Hough transformation to recognize objects with approximately 80% accuracy, but the operators are required to be familiar with the effects of object sizes and orientation on the randomized Hough transform algorithm.

2.2.2. Image-based processing

In the image-based methods using B-scan data, researchers trend to image the received waves by background removal [28] and velocity analysis [29]. For example, Chang et al. [30] tried to remove the backgrounds in the GPR images to locate reinforcing steel bars in concrete. The extended common midpoint method based on the velocity analysis, proposed in [29, 31], processes the B-scan data collected by an air-coupled antenna array to measure the thicknesses of asphalt pavements.

~~Although the imaging techniques in GPR have been calibrated with high precision based on electromagnetic properties of building materials, the utility of GPR systems still mainly depends on human experiments. Tong et al. [32] proved that the traditional methods with no human assistance could not handle the complexity foreground and background in GPR images under various real-world conditions. Therefore, It is necessary to improve these methods to handle the complex background and foreground in the GPR data and requires little experience in electromagnetic waves.~~

2.2.3. ~~Model-based processing~~

~~Recently, model-based processing techniques have~~ Image-based methods have also been applied to ~~the~~ C-scan ~~GPR data. Generally,~~ data, in which a series of 2D grid ~~images collected from a multichannel GPR , as C-scan data,~~ GPR images are transformed into 3D data~~via model-based methods~~. Compared with B-scan data, ~~the 3D~~ C-scan data can provide more space information about buried objects. However, the complexity of processing C-scans exceeds those for B-scans since the background in C-scan data is more complex [33]. For example, Klęsk et al. [34] proposed a fast analysis of C-scan data via 3D Haar-like features with the application to landmine detection. Jing and Vladimirova [33] presented a feature-based algorithm for building 3D images of buried objects using GPR signals.

~~As the model-based processing is an extension of the image-based processing, the problems introduced in Section 2.2.2 can also be found in the model-based processing techniques. In addition, the features for constructing 3D images should be provided by humans [33]~~Although the imaging techniques in GPR have been calibrated with high precision based on electromagnetic properties of building materials, the utility of GPR systems still mainly depends on human experiments. For example, Tong et al. [32] proved that the traditional methods with no human assistance could not handle the complexity background in GPR images under various real-world conditions. Therefore, It is necessary to improve these methods to handle the background in GPR data and requires little experience in electromagnetic waves.

2.3. Current Trend

From the literature review of the ~~three~~ two types of the data processing techniques, a gradual transition from unsupervised-based models (e.g., rule-driven methods) to supervised-based methods (e.g., data-driven methods) has been observed during the last few years, even though rule-driven and unsupervised studies are still important to fully understand GPR. Since 2012, more and more works are reported to address tasks involving signal processing (e.g., Jiang et

al. [35]) ~~, and~~ image processing (e.g., Higuchi et al. [36] ~~), and even 3D model analysis (e.g., and~~ Tong et al. [37]) via supervised-based methods, especially DL. The combination of DL and GPR has been the current trend in SHM.

Recently, a few review papers have indicated that it is feasible to utilize DL to process signals and images theoretically [38, 39, 40, 41]. ~~The concept and fundamental architectures of DL are first elaborated by LeCun et al [38].~~ In the review of Deng [39], the DL models are divided into three categories (generative architectures, discriminative architectures, and hybrid architectures) and their applications in signal and image are reviewed. In the work of Guo et al. [40], the architectures of convolutional neural networks (CNNs), restricted Boltzmann machines (RBMs), autoencoders, and sparse coding and their applications in signal and image are reviewed. Additionally, the timeline from artificial neural network to deep neural network is conducted by Schmidhuber [41].

Despite there are rich publications cited in the previous paragraph providing their overviews on DL, all of them present current developments of the classic issues about 1D and 2D data but do not consider any GPR case. This paper contributes to this void by reviewing the set of solutions that are based on a DL framework and providing the current issues on the set.

3. Background on Deep Learning

DL, as a subset of machine learning, attracts more and more attention after its first remarkable winning in the 2012 ImageNet challenge [8]. So far, some DL models have been constantly reported state-of-the-art performance on signal and image processing. ~~A standard DL architecture is made up of an input and an output layer with several hidden layers added between the two layers. In the several modern architectures of DL, the numbers of hidden layers are more than 10. Typical DL architectures used in the field of GPR are reviewed to make the paper more rendible for GPR researchers and engineers in this section before presenting the advances in DL with GPR in the next section.~~ In general, the DL architectures used in GPR detection can be classified to two categories based

on their outputs [39]: discriminative and generative methods. Discriminative models compute a probability distribution when given an input, while generative architectures establish an input-output joint distribution. In the application of GPR, CNNs and recurrent neural networks (RNNs) are the most popular discriminative methods, while autoencoders and deep belief neural (DBNs) are two typical examples of generative methods.

3.1. CNNs

CNNs, first proposed by LeCun et al. [42], are the most widely-used DL models in GPR and have achieved tremendous success in several fields. ~~As implied by their name, convolution operation is employed in a CNN to replace plain matrix multiplication in a traditional neural network.~~ Figure 3 presents a typical architecture of CNN, whose hidden layers are a combination of three main layers: convolution layers, pooling layers, and fully connected layers. A convolutional layer consisting of several filters is utilized to convolve the input data or the previous layer's output. The outputs of the layer then pass through a nonlinear activation layer (e.g., *ReLU* [43] and *sigmoid* [44]) and a pooling layer (e.g., stochastic pooling [45] and fractional max-pooling [46]) in sequence. The outputs of the convolutional and pooling layers stack are mapped to a high-dimension space by one or more FC layer. The mapped outputs are then imported into a classifier or a regressor layer to generate a response to the initial input data. Specific weights in each convolutional and FC layer are learned by feedforward algorithms (e.g., stochastic gradient descent [47]).

Convolutional layer is the most important structure in CNNs because of its weight sharing. It denotes that each filter is employed to convolve each patch of the input data or the previous layer's output and not just in a specific location as it happens in a traditional neural network, which reduces the model's storage requirements and improves its invariant to translation. In a GPR task, there are main two convolutional filters as shown in Figure 4. Traditional convolutional filters (illustrated in Figure 4a) are mainly used in the image processing, such as GPR B-scan images [32, 37]~~. Each filter is a square matrix with a $c \times c$ size~~

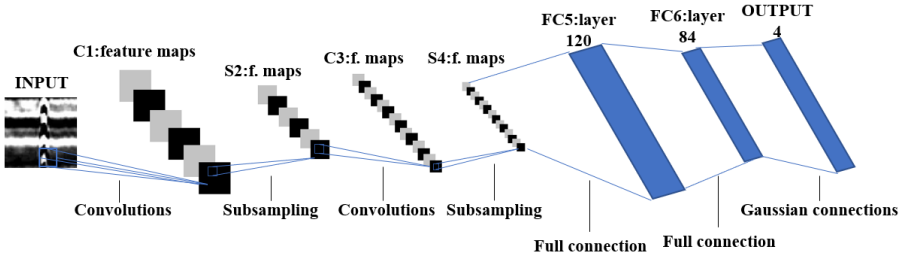

Figure 3: A typical CNN architecture for GPR [37].

~~applied to small patches of the input data in a convolutional layer. A $c \times c$ patch is called as a receptive field of the filter. Every filter is moved across the previous layer's outputs in both horizontal and vertical direction. The movement step of the filter from the top left corner to the low right corner is defined as a term "stride", whose unit is pixel. Thus, given an previous layer's output of size $o \times o$ and a filter with a $c \times c$ size and a s stride , the output size of the filter is $(o - c)/s + 1$. Another type of filter~~, while another type of filters, named one-dimension convolutional filter ~~, can be regarded as a specific form of traditional convolutional filters~~ (illustrated in Figure 4b), ~~which~~ are mainly used in the processing of GPR signals [48, 49], which can be regarded as a specific form of traditional convolutional filters. As implied by their name, the dimension of one-dimension convolutional filters is 1. In addition, their principle is the same as traditional convolutional filter.

Recently, more and more state-of-the-art techniques have reported to improve the performance of CNNs. For example, a novel convolutional layer termed as *Network in Network* [51] achieved state-of-the-art results in several classic classification tasks, such as CIFAR-10 and CIFAR-100. Generalizing pooling functions [52], layer-sequential unit-variance initialization [53], all convolutional networks [54], and so on have also been reported to improve the performance of CNNs. Unfortunately, there is little study employing these techniques for GPR systems. Thus, transfer applications of these techniques for GPR systems will be a trend to improve the performance of CNNs in future.

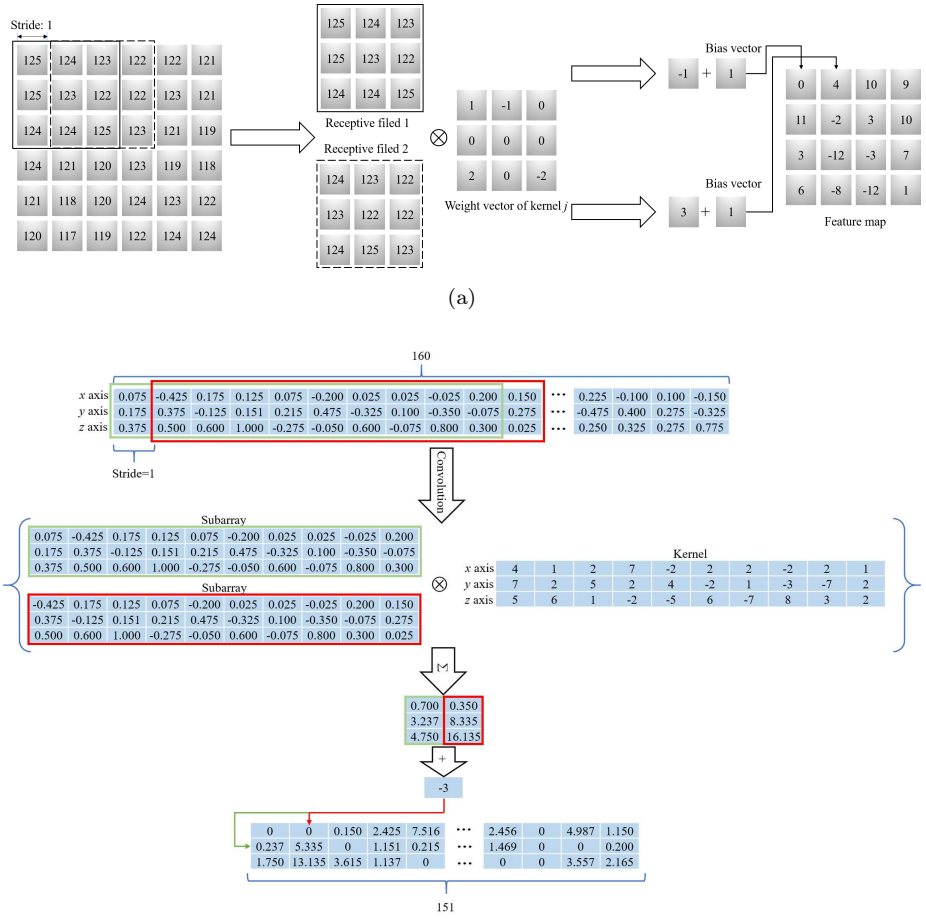

Figure 4: Examples of two main convolutional filters: (a) traditional convolutional filter [50] and (b) one dimension convolutional filter.

It will be further discussed in Section 4.4.

3.2. RNNs

RNN is another widely-used DL architecture for processing sequential data (e.g., signals [55] and sounds [56]). Each RNN consists of three weight matrices (input-to-hidden, hidden-to-hidden, and hidden-to-output) and three bias vectors (hidden, output, and the initial bias vector) [57], as shown in Figure 5. ~~An RNN iterates its hidden state over time by some nonlinearity and makes desired outputs once given input.~~ RNNs can be thought of as a series of networks linked together, such as three networks in Figure 5. They often have a chain-like architecture, in which the outputs of a network are imported into the next one. Thus, the next network outputs depend on both its inputs and the outputs of its previous network. Compared to CNNs whose inputs and outputs are independent of each other, RNNs have a "memory" which remembers all information about what has been calculated.

The remarkable performance of RNNs benefits from their ~~integration~~ "memory" capacity of iterating weights based on new information and updating the outputs. The ~~integration~~ capacity has been employed well in the processing of signal data in civil engineering. For example, Pathak et al. [58] utilized an RNN and IRT for air leakage detection in residential homes and the reported results showed the method could be used to estimate different A/C usage characteristics with 0.85 F-measure. Zhang et al. [59] present a method for pixel-level pavement crack detection via long short term memory (LSTM) and 3D NDT data.~~LSTM is a typical RNN model for processing texts and sounds and has been proved to be successful when applied for data with second-level granularity [60, 61].~~

~~Recently,~~ Recently, the applications of RNNs on the image domain have been reported and showed promising results [62, 63], and some advanced RNNs have also been used in the domain, such as LSTM [60, 61], ReNets [64], and gated RNNs [65, 66, 67, 68]. However, there is little study employing these RNNs for exploiting GPR data. Thus, transfer applications of these tech-

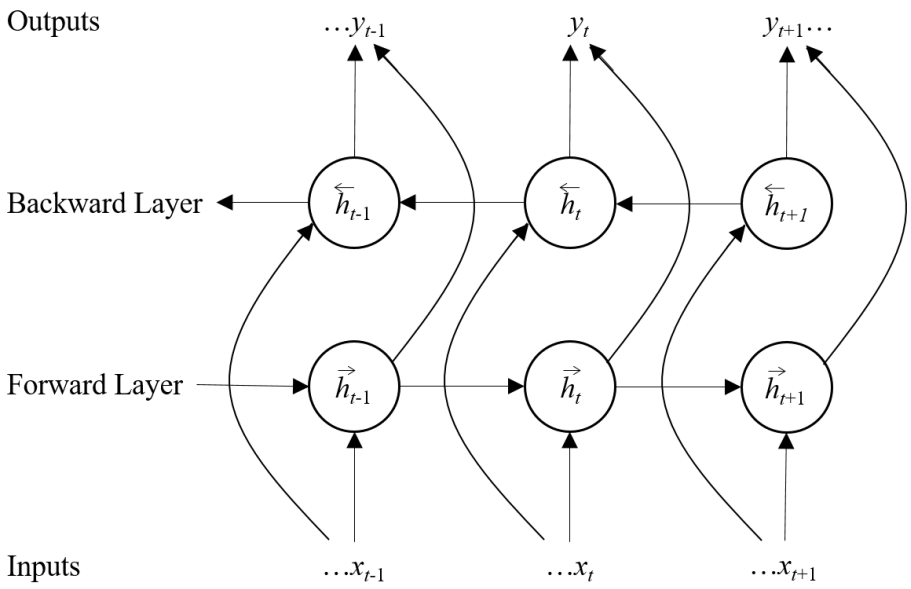

Figure 5: A typical RNN architecture [69].

niques for GPR systems may be a trend in the further years. ~~Additionally, a new RNN architecture for object recognition using images, namely ReNet, was proposed [64]. In the spatial model, several RNNs were employed to substitute all convolutional layers. Experimental results reported the ReNet have a comparable performance to CNNs and more reasonable detection capacity than LSTM [60] and gated RNN [65], two typical modified RNNs . Then this indication has later been verified by Byeon et al. [66], Yan et al. [67], and Bell et al. [68].~~

3.3. Autoencoders

Autoencoder [70] is a type of generative models. An autoencoder consists of two parts: *encoder* and *decoder*, as shown in Figure 6. The function of a encoder is to map the input data to a hidden form via weight matrixes, biases, and a nonlinear activation function (e.g., *logistic sigmoid*) , while the decoder is used to map the hidden code back to the input data resulting in a reconstruction version. The optimal weight matrixes and biases are adjusted by minimizing the

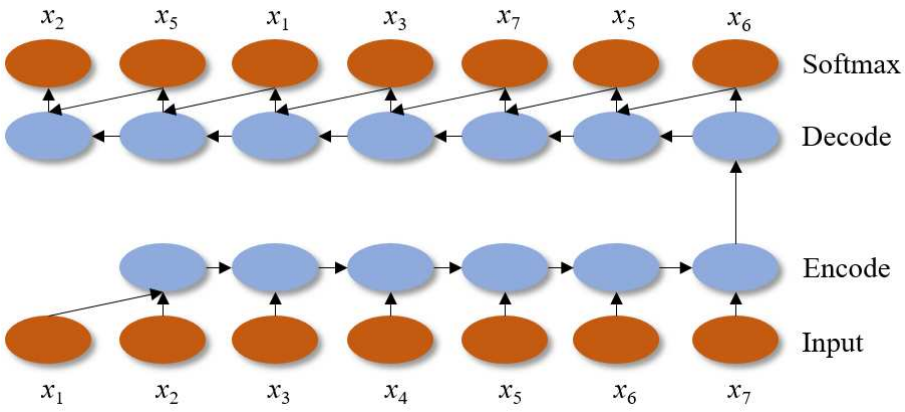

Figure 6: A typical autoencoder architecture [71].

reconstruction error, whose performance is always evaluated by a cross-entropy loss.

Autoencoders have been used for denoise and data reconstruction in the signal and image processing tasks. For example, Huang et al. [72] employed autoencoders to improve the quality of portable ultrasonic B-mode images from 32 channels to 128 channels. The simulation results revealed that the utilization of autoencoders improved the system performance, making superiority to the conventional CNNs and RNNs. Picetti et al. [73] presented a convolutional autoencoder for landmine detection and reported state-of-the-art and robust results of a wide variety of targets. Interestingly, Tong et al. [74, 75] generalized fully convolutional networks into autoencoders in the NDT for carbon fiber distribution characterization in cement-based composites.

Until recently, a large number of variants of autoencoders have been reported, such as sparse autoencoder [76], denoising autoencoder [77], and contractive autoencoder ~~. Sparse autoencoder, proposed by Boureau et al. [76], presents the possible of employing higher-dimensional but sparse representation. Denoising autoencoder [77], as a form of regularization methods, transforms corrupted data into their clean version. Contractive autoencoder [78], also as a regularization method, has been proven to perform better than the standard and denoising~~

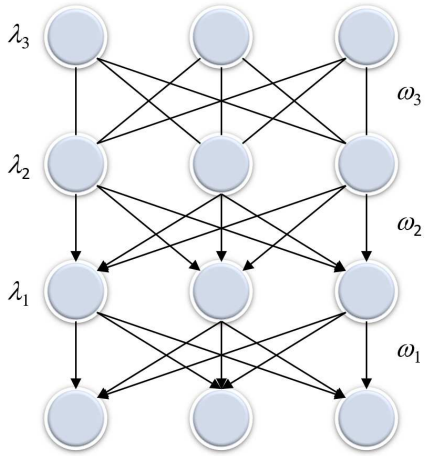

Figure 7: A typical DBN architecture [80].

~~autoencoders~~[78]. These variants show their potential in denoise and data reconstruction in the application of GPR data in civil engineering.

3.4. DBNs

DBN [79], as a type of generative models, is the first proposed DL model and have the potential to address several NDT tasks, especially in the processing B-scan data. DBNs consists of multiple layers of stochastic hidden variables [39], as shown in Figure 7. All layers in a DBN interact with directed connections except for the top two, which form an undirected bipartite graph.

As the first DL method, DBNs have been widely used in the processing of GPR signals and images. For example, Becker et al. [81] proposed a false alarm rejection method in forward-looking GPR images. The results indicated the probability of exploiting both the L-band and X-band using DBNs. Timothy et al. [82] used DBNs in forward-looking explosive hazard detection. The DBNs showed an 85% improvement in the overall detection and classification method. As learning in densely connected [83], the performance of DBNs in the NDT tasks is not as reasonable as the performance of CNNs and RNNs, though a layer-by-layer training method [84, 85] was proposed for solving the problem in some degree.

4. Advances in Deep Learning with GPR

After the huge popularity of DL in several data processing tasks, DL has been employed to exploit signal and image data in GPR systems and achieved tremendous success. In order to review this success and existing issues, we divide the existing approaches into three groups, conduct an experimental comparison among the three categories, and provide current issues: (i) The first group includes approaches using 1D raw signal data as input to the DL models (Section 4.1); (ii) The models in the second category exploit GPR images generated from raw data (Section 4.2); (iii) Deep architectures have access to exploit the 3D data form the third group (Section 4.3); (iv) State-of-the-art DL models for GPR data processing are compared (Section 4.4); and (v) The current issues of the combination between DL and GPR are discussed (Section 4.5).

4.1. DL Architectures Exploiting A-scan Data

A-scan data, as 1D amplitude-time GPR records, are the fundament of the GPR inspection. In the DL architectures exploiting A-scan data, a common practice is to approximate the low-level representations of the latent concepts related to an inspection task, then provide them as input to a deep neural network (DNN) to map useful high-level representations.

He et al. [86] extract low-level representations from the time-frequency distribution of A-scan data to represent the high-level representations related to the buried regions in the tunnels. More specially, 1200 GPR point data was first transformed by Wigner distribution to get the map of the time-frequency joint distribution. Afterward, the joint distribution was adopted to approximate the tunnel-region representations by the processing of several convolutional and pooling layers. The representations were provided as input data to a DNN for assigning the data into one of the buried region types. Experiments demonstrated the proposed method's superior performance in comparison to the support vector machine-based and DBN-based methods indicating that the high-level representations generated by the DNN are more informative and discriminative. Besides, it also implied that the CNN-based method was better than the

DBN-based method in the processing of the complex background and noise in the A-scan data. In the work of Wang [87], a stacked denoising autoencoder was adopted to extract the high-level representations under imbalanced sample conditions by a layer-by-layer greedy training method. The outputs from the first and second hidden layers of the autoencoder can be considered as the middle- and high-level representations. Afterward, the final high-level representations were imported into a classifier for human detection in the buildings. Regularization restrictions and dropout technology were also adopted. The autoencoder was considered as an unsupervised algorithm and a dimensionality reduction method. Therefore, it was compared to other unsupervised methods like the k-nearest neighbor algorithm and the J48 decision tree. The experiment results demonstrated that the extracted high-level representations from the autoencoder are more discriminative than the representations provided by humans, leading to top enhanced recognition performance.

DL architectures also have the capacity of object measurement using A-scan data. In the work of Tong et al. [88], a variant of CNN, named *Network in Network* [51], was adopted to measure the pavement defects using A-scan data. In the architecture, multilayer perceptron layers were considered as extractors to represent low-, middle-, and high-level features related to the defect shapes. The experiment results indicated that the proposed model achieved a 2.15 mm measurement error and had a distinct superiority in the effectiveness of the defect measurement. Further, Giannakis et al. [89] proposed a GPR forward solver based on DNN and A-scan, and its novelty and computational efficiency were evaluated in the application on determining the locations and diameters of reinforcement bars in concrete. More specially, the solver was made up of two sections, with each section further divided into 40 steps. The first section was used to predict the first principal axis for A-scan using neural networks. Each step could be considered as a representation of the principal component. The first section final generated a full set of predicted principal components after the 40 steps. Then the second section was designed to establish a causal relationship between the errors in the predicted values concerning the actual

principal axes and the parameters of the model. Through the numerical and real experiments, working for full-waveform inversion, it showed that the solver estimated the radius of the rebars with a maximum error of $\approx 6mm$ for the given antenna and the obtained position of the rebar and the water content of the concrete.

4.2. DL Architectures Exploiting B-scan Data

Compared with the DL architectures exploiting A-scan data, the DL models exploiting B-scan data have become more popular in the last few years. It benefits from the development of the DL frameworks (e.g., Caffe [90] and TensorFlow [91]) in the field of image processing. In general, there are mainly three directions of the DL architectures exploiting B-scan data in civil engineering: patch-based models, region-based models, and autoencoders.

In the first direction, GPR images or other B-scan data are cropped into small patches with a fixed size, which are provided as input data for a DL model in a classification task. Xiang et al. [92] adopted an improved CNN, named AlexNet, to detect rebars using small patches of GPR images. The experiment results demonstrated that AlexNet achieved a higher level of accuracy in recognizing the rebar in actually constructed facilities, though the accuracy heavily depended on the patch sizes. In the work of Tong et al. [32], a cascade CNN was proposed to recognize pavement subgrade defects using cropped GPR images. A cascade connection was used to distinguish low-resolution images from high-resolution ones. The low- and high-solution images were classified by two different CNNs. The two CNNs were trained by the low- and high-resolution datasets, respectively. The experiment results indicated the strategy using a cascade connection improved the robustness of defect recognition in low-resolution images obtained at low transmitting frequencies, though this problem was still not solved well. A deep learning-based architecture, called deep dictionary learning, was proposed to detect buried objects [93]. Each basic dictionary deep learning model was designed to calculate a Euclidean distance between a pattern and a dictionary, then all of the distances were used as representations

for classification. The computation of the Euclidean distance provided a novel thinking to solve a shortcoming of the application of DL and GPR in civil engineering, and it will be discussed in Section 4.5. In addition, in the studies of Lameri et al. [94] and Ishitsuka et al. [95], the desirable performances of patch-based methods for detecting characteristic hyperbolic signatures were reported. In general, the DL architectures have desirable performance in the classification tasks using small patches of B-scan data.

The second direction, named region-based approach, generates a region of interest (ROI) from a GPR image and assigns it into one of the classes. ~~As an~~ Compared to the first direction using cropped images with a fixed size, ROI areas in a region-based approach are flexible. As a flexible ROI is a rectangle box trying to describe an object location by its center coordinates and size, the second direction can detect objects in B-scan data more precisely than the first direction. The primary algorithms for generating an ROI are rule-driven methods. For example, in the work of Dinh et al. [96], a "*match filter*" was developed to generate potential areas surrounding rebar peaks in B-scan images and the potential areas were classified by a well-trained CNN. The results of its application on the rebars detection in twenty-six concrete bridge decks demonstrated the excellent performance of the method with an accuracy greater than 95.75%. Besaw et al. [97] extracted ROIs from the GPR B-scans by using a 2D median filter and a zeros score component analysis. The extracted ROIs were classified by a deep CNN for the buried explosive hazard detection. The reported results indicated that, given meaningful ROIs, a CNN had the capacity of classifying complex signatures contained in GPR B-scans.

With the development of deep learning, data-driven approaches raised to generate ROIs. One of the successful cases is Faster Region Convolutional Neural Network (Faster R-CNN) [98], in which a region proposal network (RPN) is designed to generate potential ROIs, and a CNN is used to classify them. Notably, the RPN and the CNN share the convolutional and pooling layers to avoid the repeating computation and reduce the running time. For example, Lei et al. [99] employed a Faster R-CNN to identify potential hyperbola

regions. More specially, a Faster R-CNN with a data augmentation strategy was used to detect rectangle regions containing traces of buried objects. Then those regions were transformed into binary images, and hyperbolic signatures in the regions were separated. Finally, downward opening hyperbola fitting was carried out using those signatures, and their respective peaks were obtained. The experiment results demonstrated that the Faster R-CNN had the desirable performance on extracting ROIs from the GPR B-scan autonomously and efficiently, which had the potential in the analysis of synthetic and on-site GPR data sets. Xu et al. [100] improved the Faster R-CNN framework by feature cascade, adversarial spatial dropout network, and soft-nonmaximum suppression for the railway subgrade defect detection. Feature cascade means that the low-, middle-, and high-level representations are combined to form new multi-sized features. It has been proved useful for detecting small objects [101]. The adversarial spatial dropout network can be considered as a learning strategy for generating hard positive samples to reduce the unbalance in the B-scans dataset. In the soft-nonmaximum suppression, the confidence levels of bounding boxes are reduced according to their overlapping area instead of directly suppressing the boxes whose confidence levels are higher than a threshold. The detecting results showed that the improved Faster R-CNN achieved an mAP of 83.6% for subgrade defect detection, which was higher than the mAP of the baseline Faster R-CNN. In addition, a comparison study demonstrated the superiority of the proposed model on the robustness to the baseline Faster R-CNN thanks to the three improvements. In the work of Pham et al. [102], the success of a Faster R-CNN on buried objects detection using GPR images is also reported.

In general, we find that the data-driven algorithms for region-based models outperform the rule-driven algorithms. This is because the rules provided by humans for ROI extraction are always not as complete as the knowledge summarized from a big dataset by a data-driven algorithms. Unfortunately, as the work principles of data-driven algorithms (e.g., neural network) are still described as a "*black box*", these knowledge cannot be summarized as some forms easy for humans to understand. The development of the explanation of "*black*

box" [103] may be helpful to generate the understandable rule to identify hyperbola regions. In the future, it is potential to transform this knowledge into rules to facilitate the GPR system, even promote the ~~developement of Maxwell's equations and constitutive relationships (Eq. ?? and ??)~~ development of the use of Fresnel law, which governs EM wave reflection and refraction.

The third direction based on autoencoder is to map GPR B-scan data to more clear descriptions, in which the objects are easier to be interpreted and detected. Alvarez and Kodagoda [104] proposed an autoencoder network to interpret the real shapes and locations of the buried objects based on the B-scan data of synthetic aperture radars. The architecture of the proposed network can be divided into two part: (a) an encoder used to downsample and compress the B-scan data to the latent representations, and (b) an decoder designed to transform the representations to sub-surface permittivity maps, in which the shapes and locations of the buried objects can be interpreted easily. The evaluation results indicated that the autoencoder network achieved a 0.7782 structural similarity index between the network outputs and the ground truths. Structural similarity index is a widely-used metric for measuring the pixel-level difference between two images [105]. Besides, the comparison results demonstrated the autoencoder's superiority in the effectiveness and simplicity over other state-of-the-art deep learning architectures, such as conditional adversarial network and U-net. In the work of Picetti et al. [73], three different autoencoder architectures were developed to provide a novel description of B-scans, in which landmine trances were considered as anomalies. The three architectures $\mathcal{N}_1 - \mathcal{N}_3$ are symmetric but have different convolutional filters. In the experiments, the receiver operating characteristic (ROC) curves, representing the probability of correct and false detection by spanning all possible values of a threshold Γ, were used to compare the performance of $\mathcal{N}_1 - \mathcal{N}_3$. The ROC results demonstrated that optimal architecture $\mathcal{N}_1$ can represent the landmine areas as an anomaly.

4.3. DL Architectures Exploiting C-scan Data

C-scan GPR data, obtained from a multichannel GPR system, can be considered as a space combination of several B-scan data. Although C-scan data are more informative, there are only a small number of studies exploiting C-scan data using DL owing to the complexity of the C-scan GPR data and the limitation of the DL architectures exploiting 3D data [80].

Kim et al. [106] proposed a DL-based method for underground object classification using C-scan GPR data. More specially, 3D GPR signals collected by a multichannel GPR system are first cropped by a 3D window box. Then, B-scan and C-scan images are extracted from the cropped 3D data. These B-scan images and C-scan slides are transformed into a 2D orthogonal grid map, which is used as input data for a deep CNN for buried object classification. In the experiment of the field data collected from urban roads, the performance of the proposed method was better than the traditional methods only using B-scan data in the classification of cavities, pipes, manholes, and subsoil background. It indicated that the C-scan GPR data contained more information concerning the class membership than the B-scan data. Similarly, in the work of Tong et al. [37], 3D GPR data was transformed into 2D data, and a CNN-based model used these 2D data for feature point extraction. These feature points were used to describe the contour profiles of pavement cracks for its 3D reconstruction. It can be found that the main idea of these methods is to transform the 3D data into 2D data. The transformation always leads to information losses. Thus, the utilization of the state-of-the-art DL architectures exploiting 3D data directly can be a way to solve the problem.

4.4. Overview and Comparison of the DL Architectures

In the past decade, DL models have been designed and successfully applied to three types of GPR data. In order to further understand these models, the works described in Section 4.1 - 4.3 are compared using a pavement GPR dataset. The dataset was collected from four highways in China using two transmitting frequencies 300 MHz and 1.2 GHz. Two types of pavement defects

(cracks and uneven settlements) are labeled. Complete information can be found in *Data Availability*. The comparison study only presents a fair competition of these DL architectures in the pavement defect detection. More works can be performed in the future ~~in the further~~ to compare the performance of these DL architectures in the entire field of civil engineering. Table 1 summarizes typical cited works, classifies them into the types of the input data, and presents the DL architectures along with some necessary details~~and two evaluation indexes (~~. Two metrics, classification accuracy and intersection over union (IoU), are used to evaluate the performance of deep-learning models in pavement defect detection. Classification accuracy is the percent of defects in a GPR dataset that are correctly classified, while IoU is to take the ratio of the intersection between predicted results and ground truth labels over the union between these two sets. Thus, classification accuracy and ~~location error)~~IoU are used to evaluate the performance of the deep-learning models in defect recognition and location, respectively. From Table 1, we can find:

- Compared with the architectures exploiting B- and C-scan, the ones exploiting A-scan have a slight advantage ~~for the pavement defect detection~~ in defect class recognition and location computation. It is because some necessary pre-processing (e.g., filtering and information compress) is conducted on GPR data for the utilization of B- and C-scan as the input. These pre-processing procedures sometimes lead to feature and information loss. In the DL architecture using A-scan data, the raw GPR signals are directly used as inputs, which reserve all useful and useless information. Considering the DL's powerful capacity of filtering features not related to the detection task, the useless information in the input has limited effects on the final performance.

- ~~DL architectures exploiting~~ We should also consider the integrity of scanning information when choosing DL algorithms. For example, the information retrieved from A-Scans is localized while C-Scans provide a three-dimensional map, even though the DL architectures exploiting A-scans trend to use

several sequent signals to improve their representativeness. Thus, DL architectures exploiting C-scan are the most promising, though their performances now are not as desirable as the performance of the architectures exploiting A-scan. Compared with A- and B-scan data, C-scan data contains complete space information of concealed defects in the pavements. It means more representations and features can be extracted from C-scan data than A- and B-data, which are essential to further improve the performance of DL architectures exploiting GPR data. Unfortunately, to our best knowledge, now no DL architectures use C-scan data without preprocessing procedures. The state-of-the-art DL architectures [80] should be considered to exploit C-scan data directly in the future.

- ~~Some fundamental~~ RNNs outperform CNNs and autoencoders in the use of A-scan data because of their temporal dynamic behavior. This indicates that RNNs can take the input data sequence into account, while CNNs and autoencoders are not. The sequence of input data, especially A-scan data, is an essential feature of GPR data.

- Some techniques are useful and essential for improving the precision and generalization of DL architectures exploiting GPR data. The first is data augmentation, including cropping, rotating, and flipping input images. It can reduce overfitting and improve the generalization of DL architectures because it can be considered as noises in the training. A gradient descent algorithm tends to balance the negative effects of the noise to minimize the overall error. In practice, this type of noise is common, such as object incline, rotation, and angulation. Another is prior knowledge, such as hand-crafted features and transfer learning. It can increase the training effectiveness because the pre-training phase is compressed. We also find that data-driven features from transfer learning work better than hand-crafted features because the prior knowledge learning from a desirable data set is better than the one provided by humans. In addition, dictionary learning and spatial dropout also have positive effects on DL's performance.

4.5. Current Issues

From the literature review and the comparison study, we find two inherent defects of DL limiting its application on exploiting GPR data: (a) the dependence on the big data for training a desirable DL model, and (b) the arbitrary decision-making of DL model for classification tasks.

4.5.1. Dependence on big data

It has been widely known that the performance of a DL model heavily depends on the quality of its learning dataset. Insufficient sample number, sample unbalance among the class membership, and label corrosion always lead a poor capacity of a DL model, such as overfitting, low generality, and unacceptable robustness. Unfortunately, GPR datasets for training a DL model are not as ample as the benchmark datasets for developing a DL model to solve classic issues, such as the CIFAR-10 [109], ImageNet [110], and "For Music Analysis" [111] datasets. Many previous studies mentioned in Section 4.1 - 4.3 reported that their DL models were trained by a small number of GPR-data samples, less than 10^4. To make matters worse, the unbalance in these GPR datasets is inevitable because some data are not easy to collect in practice.

Now, there are main three solutions to the issue. The first solution is the use of transfer learning in the pre-training phase. Transfer learning is a technique applying the knowledge acquired while solving one issue to a different but related problem. In the work of Bralich et al. [112] and Reichman et al. [113], the prior knowledge learning from the CIFAR-10 dataset was transferred to the CNN model for buried target detection in the pre-training phase. Then the pre-trained CNN model is fine-tuned by a small GPR dataset. In the study of Enver and Yüksel [114], the learned weights in the imagenet-matconvnet-vgg-f model trained on the Imagnet Large Scale Visual Recognition Challenge (ILSVRC 2012) data [115] was transformed to a CNN for buried wire detection. Unfortunately, a transfer learning strategy can only help a DL model learn some low-level representations from these benchmark datasets, such as lines and gray scales. This is because the latent middle- and high-level representations related

Table 1: A Comparison Study of DL Architectures Exploiting GPR data

Input	Method	Deep model	Key techniques	CA/%	IoU
A-scan	He et al. [86]	CNN	Wigner distribution	82.43	0.8212
	Wang et al. [87]	Autoencoder	Greedy learning Regularization restrictions	83.67	0.8320
	Tong et al. [88]	CNN	Network in network Cascade connection	85.17	0.8404
	Giannakis et al. [89]	DNN	PPCA training method GPR dataset from FDTD	84.26	0.8512
	Haşim et al. [55]	RNN	Long short-term memory	84.26	0.8626
B-scan	Xiang et al. [92]	CNN	AlexNet	76.28	0.6755
	Umut and Levent [93]	DBN	Dictionary learning	80.31	0.6962
	Lameri et al. [94]	CNN	Hand-crafted feature	80.76	0.7233
	Kyle and Sarath [104]	Autoencoder	DSSIM loss	77.32	0.7148
	Francesco et al. [73]	Autoencoder	Undercomplete convolutional layer	78.46	0.6882
	Kien et al. [96]	CNN	Normalized cross correlation Thresholding	75.69	0.6420
	Besaw and Stimac [97]	CNN	Hand-crafted feature	76.42	0.6682
	Gao et al. [107]	Faster R-CNN	Data augmentation	82.57	0.8491
	Pham and Sébastien [102]	Faster R-CNN	Transfer learning GPR dataset from FDTD	80.43	0.8002
	Xu et al. [100]	Faster R-CNN	Data augmentation Feature cascade	81.62	0.8134
	Pau et al. [108]	RNN	Long short-term memory	81.62	0.8332
C-scan	Tong et al. [37]	CNN	Feature point extraction Cascade connection	78.43	-
	Kim et al. [106]	CNN	Grid transformation	80.12	-

Here: PPCA = predictive principal component analysis technique, FDTD = Finite-Difference Time-Domain, DSSIM = structural dissimilarity; CA=classification accuracy; IoU=intersection over union.

to the class membership in these benchmark datasets are very different from the targets in GPR data, such as outlines and waveforms. In addition, there are commonly two different and distinct phases in the training of DL: pre-training and fine-tuning. Schwartz-Ziv and Tishby [116] indicated that the fine-tuning phrase could be considered as compressing the internal representations under the training error constraint, which is mainly responsible for the absence of overfitting in DL. Thus, we can conclude that transfer learning in the pre-training phase has limited help for the problem because the procedure of compressing low-level representations to middle- and high-level representations in the fine-tuning phase still raises overfitting owing to the lack of training samples.

The second solution is semi-supervised learning. It means that humans provide some hand-crafted representations before training a DL-model. For example, Malof et al. [117] proposed to construct a CNN architecture that closely emulates successful hand-crafted feature designs for GPR buried object detection. The experiment results indicated the feasibility and effectiveness of this approach for training a DL-model. However, the problem is that it is not easy for humans to summary all useful representations related to the buried object detection formally, especially high-level representations.

The third approach is to enlarge the dataset using simulation data or data augmentation. In the works of Pham et al. [102] and Sonoda and Kimoto [118], thousands of GPR images were generated using finite-difference-time-domain simulation. Veal et al. [119] proposed a generative adversarial network-based method to impute new data based on limited and class imbalance GPR data. These works reported improvement of accuracy and robustness because of the reduction of class and condition unbalance in the training datasets. Unfortunately, a problem still exists that the developed DL model has undesirable stability on noises and backgrounds. This is because the simulation conditions are simpler than the real-world conditions, especially noise patterns and electromagnetic properties and distributions of the mediums. In addition, data augmentation, as a widely-used technique to avoid overfitting [120], is also used to reduce the dependence of big data in the GPR DL architectures, such as the

study of Reichman et al. [113], though it has limited help to solve the problem of the class imbalance.

In summary, from the findings of this section, we can conclude that the dependence of big data in the training of DL architectures exploiting GPR data is still not solved well because of the limitations of the three solutions. As a large number of the publications reported their well-developed CNN for exploiting GPR data, we think the optimal solution for the problem is to share the data from the GPR researchers in the world to build a benchmark GPR dataset. The similar works are standard in the field of deep learning [109, 110, 111], even computer science, but cannot be found in the field of NDT. As a pioneer, we provide our GPR dataset of pavement defect inspection used in Section 4.4. It is the first step for our proposed solution.

4.5.2. Arbitrary decision-making of DL models

As for the second inherent defects of DL, we would like to explain it starting ~~from~~ with defining DL as a prediction function $\widehat{F}: \mathcal{X} \mapsto \mathcal{Y}$ with a minimum error $\sum_{Y_i \neq \widehat{F}(X_i)} E\left(Y_i, \widehat{F}(X_i)\right), i = 1, \ldots, n$, once given a learning set $\chi = \{(X_1, Y_1), \ldots, (X_n, Y_n)\}$, where $\mathcal{X}$ is a p-dimension representation space $\mathbb{R}^p$; $\mathcal{Y}$ is a assignment space $\{y_1, \ldots, y_k\}$ with k class; and ~~$E(\cdot)$~~ $E()$ is a cost function. For a new sample with an input-label pair (x, y), a DL model describes the new sample as an estimate of a conditional distribution $\widehat{F}(x) = \{p_1(y_1|x), \ldots p_k(y_k|x)\}$ and assign it to class y_a with $a = \max_{j=1,\cdots,k} p_j(y_j|x)$. This often results a *hubristic bias*: overconfidence in the assignment of a definite class [121]. Exactly, a DL model is forced to assign the new sample to one of the k classes, even though its input x includes some conflict and confusing information. For example, x provides confusing information indicating the DL model should classify the sample to y_1 or y_2 but cannot make a precision decision between the two classes. However, no existing DL can perform it. Additionally, conflict information exists if the sample includes two or more classes, such as a B-scan GPR image with two types of pavement distresses. However, traditional DL models ignore conflict information and make a arbitrary decision.

This problem should not be neglectful in the applications of DL in GPR for civil engineering. As discussed in Section 4.5.1, the observations in a GPR dataset usually are concentrated on a small volume. Still, a DL architecture is expected to provide definite predictions for the entire space. For instance, some buried objects are made of different materials but have the same shape, which are difficult to distinguish from GPR images as their signatures look very similar. The same object buried in different soils shows different signatures in a GPR image. In addition, some detection objects usually exist in the same area, which means an abnormal signal in A-scan data or a hyperbolic signature from a B-scan image may contain information representing more than one object. Therefore, the *hubristic bias* raises a problem of arbitrary decision-making.

One approach to solve this problem is to fuse the data from different sources to make a decision. In the work of Sakaguchi et al. [122], three strategies for fusing data from L-band and LIDAR GPR were proposed. The first strategy is data-level fusion, where the two types of data are stacked and used as input data, while the second one is also data-level fusion, which is realized by concatenating the side of the images by the side. The final one is feature-level fusion, in which the output features from two CNNs were concatenated one by one for classification. The experiment results indicated that the second strategy achieved the best performance for the buried object detection, while the worst performance was from the third one. The authors imputed it to the poor optimization owing to the additional parameters in the third model. However, we believe that the third strategy is promising if a desirable fusion method is adopted instead of the simple concatenation, such as Dempster-Shafer theory [123] and contextual reliability evaluation [124].

Another approach is to design cautious or evidential classifiers for exploiting GPR data. A cautious or evidential classifier means it can provide imprecise and ambiguous classification, such as assigning a sample to a multi-class set $\{y_1, y_2\}$ or making a rejection decision, while a traditional DL algorithm can only make a precise classification. The assignment to a multi-class set $\{y_1, y_2\}$ means that a classifier believes a sample belongs to class y_1 or y_2 but do not

know which one, while rejection indicates that the classifier does not know which class the sample belongs to. Yotam et al. [125] proposed cautious deep learning allowing for ambiguous rejection by replacing $p(y_j|x)$ with $p(x|y_j)$ since $p(y_j|x) = p(x|y_j)p(y_j)/p(x)$ the prediction involves the balance between between $p(y_j)$ and $p(x|y_j)$, $j = 1, \ldots, k$. More specially, the method first finds an estimate $\widehat{p}(x|y_j)$ of $p(x|y_j)$ and an appropriate scalar $\widehat{t}_y$. Then the method assigns the sample x to class y_j iff $C(x) = \{y_j | \max_{j=1,\cdots,k} p_j(y_j|x) > \widehat{t}_y\}$. Otherwise, the method makes ambiguous rejection. In practice, only in the special case that all of the k classes have the same probability $p(y_j)$ in the real-world conditions, the negative effects of $p(y_j)$ on $p(y_j|x)$ can be ignored. However, in the GPR detection for civil engineering, the frequencies of different buried objects are obviously different. For example, the number of cracks is much more than the number of uneven settlements in a pavement. Thus, $p(y_a)$ are different from $p(y_b)$ for y_a and $y_b \in \{y_1, \ldots, y_k\}$. Therefore, there are significant advantages to use $p(x|y_j)$ to build a DL classifier for exploiting GPR data by taking $p(y_j)$ into account and tieing the prediction of an observation x with the likelihood of observing that class.

Tong et al. [126] proposed a distance-based DL allowing for ambiguous rejection, called ConvNet-BF classifier or evidential DL. In the method, the distances between a pattern x and some prototypes are computed and used to build mass functions based on Dempster-Shafer theory. The mass functions are used for assigning the sample to one of the classes or rejecting based on an evidence-theoretic rule [127]. Interestingly, ~~a~~ ConvNet-BF ~~classifier can be combined with one of the~~ classifiers can make set-valued assignments [128], which are a subclass of imprecise classification. A set-valued decision ~~strategies to assign~~ is defined as assigning a sample to ~~a multi-class set [128]~~one of the non-empty subsets in the assignment space $\{y_1, \ldots, y_k\}$. For example, a ConvNet-BF classifier has capacity of assigning a sample to set $\{y_1, y_2\}$ if conflict information exists in the sample. It seems to have the generalized potential to solve the problem of the arbitrary decision-making of DL models. From the view of the GPR detection for civil engineering, the proposed method can ~~provide a~~ perform multi-class predic-

tion when two or more detection objects exist in the same area. ~~It~~ Multi-class prediction is a assignment to a non-empty subset whose cardinality is larger than one. ConvNet-BF classifier can also indicate the uncertainty from GPR data (e.g., the same object buried in different areas showing different signatures in GPR data) using its additional output mass functions $m(\Omega)$. The conflicts in GPR data can be characterized by two near values of output mass functions (e.g., two different types of the buried objects with similar signatures from G-PR data). The maximal conflict corresponds to $m(\{y_i\}) = m(\{y_j\}) = 0.5$. For complete introduction, readers are invited to refer to Denœux's original work [129] and its extension to DL [126]. However, little has been done to combine recent techniques of cautious and evidential DL with GPR data. It will be an important issue for the combination of GPR and DL for civil engineering.

5. Conclusions

The progressive evolution of GPR techniques with desirable capabilities poses unique chances, as well as new challenges, to NDT for civil engineering. DL managed to revolutionize many classification and regression tasks achieving or even exceeding the human-level precision, and it currently began to be employed in the field of GPR. Even though GPR devices provide precise and stable representations of buried objects and backgrounds, its intricate data structure leads the exploitation using DL architectures not easy. In this survey, we divided DL architectures exploiting GPR data into three groups from the view of the scanning types of GPR. In general, the experiment results indicated a slight advantage of DL architectures exploiting A-scan data for the GPR detection in comparison to those using B-scan images. The recent works managed to achieve promising performance utilizing C-scan data; however, more complex architectures or pre-processing procedures were required.

The dependence of big data, a current research issue of combining DL and GPR for civil engineering detection, is currently attracting a lot of interest. ~~Transfer~~ There are three directions to reduce the dependence, transfer learning,

semi-supervised learning based on hand-crafted representations, and enlargement a dataset using simulation data or data augmentation~~can lead to faster convergence and reduce the dependence of big data, though~~ . However, the possibility of overfitting and low generalization are still not solved well owing to a small volume of the real observations in a GPR dataset~~are still not solved well~~. The optimal solution for the problem is to share the data from the GPR researchers in the world to build a benchmark GPR dataset. Another current research problem is the arbitrary decision-making of DL models raised by its overconfidence in assigning a GPR sample to a definite class. Fusing data from different types of GPR devices, even other NDT techniques, is an effective solution. In addition, novel evidential DL has the generalized potential to solve the problem. From the view of the GPR detection for civil engineering, an evidential DL architecture can provide a multi-class and imprecise prediction when conflict and uncertainty exist in GPR data. However, little has been done to combine evidential DL techniques with GPR data. It will be an essential issue for the application of DL on GPR detection for civil engineering.

Data Availability

All GPR data used in Section 4.4 in the form of B-scan are available in Googly Drive via Developing GPR data set.

Acknowledge

Authors unfeignedly thanks Googly Colaboratory for its support in the comparison study. This work is also supported by the co-operation Program with the UTs and INSAs (France) funded by the China Scholarship Council (No. CSC201801810108) and science and technology research project of Jiangxi Provincial Department of Education (Grant No. GJJ190361).

References

[1] K. Ito, K. Xiong, Gaussian filters for nonlinear filtering problems, IEEE Transactions on Automatic Control 45 (5) (2000) 910–927. doi:10.1109/9.855552.

[2] C. Silpa-Anan, R. Hartley, Optimised kd-trees for fast image descriptor matching, in: 2008 IEEE Conference on Computer Vision and Pattern Recognition, IEEE, Anchorage, AK, USA, 2008, pp. 1–8. doi:10.1109/CVPR.2008.4587638.

[3] D. Marcos, M. Volpi, D. Tuia, Learning rotation invariant convolutional filters for texture classification, in: 2016 23rd International Conference on Pattern Recognition (ICPR), IEEE, Cancun, Mexico, 2016, pp. 2012–2017. doi:10.1109/CVPR.2008.4587638.

[4] N. Kanopoulos, N. Vasanthavada, R. L. Baker, Design of an image edge detection filter using the sobel operator, IEEE Journal of Solid-State Circuits 23 (2) (1988) 358–367. doi:10.1109/4.996.

[5] P. Demartines, J. Hérault, Curvilinear component analysis: A self-organizing neural network for nonlinear mapping of data sets, IEEE Transactions on Neural Networks 8 (1) (1997) 148–154. doi:10.1109/72.554199.

[6] L. Zhang, W. Zhou, L. Jiao, Wavelet support vector machine, IEEE Transactions on Systems, Man, and Cybernetics, Part B (Cybernetics) 34 (1) (2004) 34–39. doi:10.1109/TSMCB.2003.811113.

[7] J. F. Sham, W. W. Lai, Development of a new algorithm for accurate estimation of GPR's wave propagation velocity by common-offset survey method, NDT & E International 83 (2016) 104–113. doi:10.1016/j.ndteint.2016.05.002.

[8] A. Krizhevsky, I. Sutskever, G. E. Hinton, Imagenet classification with deep convolutional neural networks, in: Advances in Neural Information

Processing Systems 25, Curran Associates, Inc., 2012, pp. 1097–1105. doi:10.1145/3065386.

[9] W. S. McCulloch, W. Pitts, A logical calculus of the ideas immanent in nervous activity, The Bulletin of Mathematical Biophysics 5 (4) (1943) 115–133. doi:10.1007/BF02478259.

[10] F. Rosenblatt, The perceptron: a probabilistic model for information storage and organization in the brain, Psychological Review 65 (6) (1958) 386. doi:10.1037/h0042519.

[11] R. M. Morey, Ground penetrating radar for evaluating subsurface conditions for transportation facilities, Transportation Research Board, 1998.

[12] A. Benedetto, G. Manacorda, A. Simi, F. Tosti, Novel perspectives in bridges inspection using GPR, Nondestructive Testing and Evaluation 27 (3) (2012) 239–251. doi:10.1080/10589759.2012.694883.

[13] A. Benedetto, L. Pajewski, Civil engineering applications of ground penetrating radar, Springer, 2015. doi:10.1007/978-3-319-04813-0.

[14] I. L. Al-Qadi, S. Lahouar, Use of GPR for thickness measurement and quality control of flexible pavements, Journal of the Association of Asphalt Paving Technologists 73 (2004) 501–528.

[15] P. Gamba, S. Lossani, Neural detection of pipe signatures in ground penetrating radar images, IEEE Transactions on Geoscience and Remote Sensing 38 (2) (2000) 790–797. doi:10.1109/36.842008.

[16] M. Ramírez-Blanco, F. García-García, I. Rodríguez-Abad, R. Martínez-Sala, J. Benlloch, Ground-penetrating radar survey for subfloor mapping and analysis of structural damage in the sagrado corazón de jesús church, spain, Archaeological prospection 15 (4) (2008) 285–292. doi:10.1002/arp.341.

[17] J. Davis, A. P. ANNAN, Ground-penetrating radar for high-resolution mapping of soil and rock stratigraphy 1, Geophysical prospecting 37 (5) (1989) 531–551. doi:10.1111/j.1365-2478.1989.tb02221.x.

[18] J. Huisman, C. Sperl, W. Bouten, J. Verstraten, Soil water content measurements at different scales: accuracy of time domain reflectometry and ground-penetrating radar, Journal of Hydrology 245 (1-4) (2001) 48–58. doi:10.1016/S0022-1694(01)00336-5.

[19] A. Benedetto, F. Tosti, Inferring bearing ratio of unbound materials from dielectric properties using GPR: the case of runaway safety areas, in: Airfield and Highway Pavement 2013: Sustainable and Efficient Pavements, 2013, pp. 1336–1347. doi:10.1061/9780784413005.113.

[20] F. Tosti, S. Adabi, L. Pajewski, G. Schettini, A. Benedetto, Large-scale analysis of dielectric and mechanical properties of pavement using GPR and LFWD, in: Proceedings of the 15th International Conference on Ground Penetrating Radar, IEEE, Brussels, Belgium, 2014, pp. 868–873. doi:10.1109/ICGPR.2014.6970551.

[21] N. Economou, A. Vafidis, Spectral balancing GPR data using time-variant bandwidth in the t-f domain, Geophysics 75 (3) (2010) J19–J27. doi:10.1190/1.3374464.

[22] L. Nuzzo, Coherent noise attenuation in GPR data by linear and parabolic radon transform techniques, Annals of Geophysics 46 (3). doi:10.4401/ag-3426.

[23] D. J. Daniels, Ground Penetrating Radar, American Cancer Society, 2005. doi:10.1002/0471654507.eme152.

[24] H. M. Jol, Ground penetrating radar theory and applications, elsevier, Amsterdam, Netherlands, 2008. doi:10.1016/B978-0-444-53348-7.00016-8.

[25] P. Shangguan, I. Al-Qadi, A. Coenen, S. Zhao, Algorithm development for the application of ground-penetrating radar on asphalt pavement compaction monitoring, International Journal of Pavement Engineering 17 (3) (2016) 189–200. doi:10.1080/10298436.2014.973027.

[26] S. Zhao, P. Shangguan, I. L. Al-Qadi, Application of regularized deconvolution technique for predicting pavement thin layer thicknesses from ground penetrating radar data, NDT & E International 73 (2015) 1–7. doi:10.1016/j.ndteint.2015.03.001.

[27] W. Li, X. Cui, L. Guo, J. Chen, X. Chen, X. Cao, Tree root automatic recognition in ground penetrating radar profiles based on randomized hough transform, Remote Sensing 8 (5) (2016) 430. doi:10.3390/rs8050430.

[28] Q. Dou, L. Wei, D. R. Magee, A. G. Cohn, Real-time hyperbola recognition and fitting in GPR data, IEEE Transactions on Geoscience and Remote Sensing 55 (1) (2016) 51–62. doi:10.1109/TGRS.2016.2592679.

[29] Z. Leng, I. L. Al-Qadi, An innovative method for measuring pavement dielectric constant using the extended cmp method with two air-coupled GPR systems, NDT & E International 66 (2014) 90–98. doi:10.1016/j.ndteint.2014.05.002.

[30] C. W. Chang, C. H. Lin, H. S. Lien, Measurement radius of reinforcing steel bar in concrete using digital image GPR, Construction and Building Materials 23 (2) (2009) 1057–1063. doi:10.1016/j.conbuildmat.2008.05.018.

[31] S. Zhao, I. L. Al-Qadi, Development of an analytic approach utilizing the extended common midpoint method to estimate asphalt pavement thickness with 3-d ground-penetrating radar, NDT & E International 78 (2016) 29–36. doi:10.1016/j.ndteint.2015.11.005.

[32] Z. Tong, J. Gao, H. Zhang, Innovative method for recognizing subgrade defects based on a convolutional neural network, Construction and Building Materials 169 (2018) 69–82. doi:10.1016/j.conbuildmat.2018.02.081.

[33] H. Jing, T. Vladimirova, Novel algorithm for landmine detection using C-scan ground penetrating radar signals, in: 2017 Seventh International Conference on Emerging Security Technologies (EST), IEEE, Canterbury, UK, 2017, pp. 68–73. doi:10.1109/EST.2017.8090401.

[34] P. Klęsk, A. Godziuk, M. Kapruziak, B. Olech, Fast analysis of C-scans from ground penetrating radar via 3-D haar-like features with application to landmine detection, IEEE Transactions on Geoscience and Remote Sensing 53 (7) (2015) 3996–4009. doi:10.1109/TGRS.2015.2388713.

[35] J. Jiang, Z. Zhang, Q. Dong, F. Ni, Characterization and identification of asphalt mixtures based on convolutional neural network methods using X-ray scanning images, Construction and Building Materials 174 (2018) 72–80. doi:10.1016/j.conbuildmat.2018.04.083.

[36] Y. Higuchi, T. Babasaki, Failure detection of solar panels using thermographic images captured by drone, in: 2018 7th International Conference on Renewable Energy Research and Applications (ICRERA), IEEE, Paris, France, 2018, pp. 391–396. doi:10.1109/ICRERA.2018.8566833.

[37] Z. Tong, J. Gao, H. Zhang, Recognition, location, measurement, and 3D reconstruction of concealed cracks using convolutional neural networks, Construction and Building Materials 146 (2017) 775–787. doi:10.1016/j.conbuildmat.2017.04.097.

[38] Y. LeCun, Y. Bengio, G. Hinton, Deep learning, Nature 521 (7553) (2015) 436. doi:10.1038/nature14539.

[39] L. Deng, A tutorial survey of architectures, algorithms, and applications for deep learning, APSIPA Transactions on Signal and Information Processing 3 (2014) E2. doi:10.1017/atsip.2013.9.

[40] Y. Guo, Y. Liu, A. Oerlemans, S. Lao, S. Wu, M. S. Lew, Deep learning for visual understanding: A review, Neurocomputing 187 (2016) 27–48. doi:10.1016/j.neucom.2015.09.116.

[41] J. Schmidhuber, Deep learning in neural networks: An overview, Neural Networks 61 (2015) 85–117. doi:10.1016/j.neunet.2014.09.003.

[42] Y. LeCun, L. Bottou, Y. Bengio, P. Haffner, et al., Gradient-based learning applied to document recognition, Proceedings of the IEEE 86 (11) (1998) 2278–2324. doi:10.1109/5.726791.

[43] V. Nair, G. E. Hinton, Rectified linear units improve restricted boltzmann machines, in: Proceedings of the 27th international conference on machine learning (ICML-10), Haifa, Israel, 2010, pp. 807–814.

[44] X. Glorot, Y. Bengio, Understanding the difficulty of training deep feedforward neural networks, Journal of Machine Learning Research - Proceedings Track 9 (2010) 249–256.

[45] M. D. Zeiler, R. Fergus, Stochastic pooling for regularization of deep convolutional neural networks (2013). arXiv:1301.3557.

[46] B. Graham, Fractional max-pooling (2014). arXiv:1412.6071.

[47] L. Bottou, Large-scale machine learning with stochastic gradient descent, in: Proceedings of COMPSTAT'2010, Springer, Heidelberg,German, 2010, pp. 177–186. doi:10.1007/978-3-7908-2604-3_16.

[48] K. Virupakshappa, M. Marino, E. Oruklu, A multi-resolution convolutional neural network architecture for ultrasonic flaw detection, in: 2018 IEEE International Ultrasonics Symposium (IUS), IEEE, Kobe, Japan, 2018, pp. 1–4. doi:10.1109/ULTSYM.2018.8579888.

[49] J. Tan, D. Xia, S. Dong, B. Xu, Y. Liang, H. Zhu, E. Li, Research on joint nondestructive testing based on neural network, in: Intelligent Computing

and Internet of Things, Springer, Singapore, 2018, pp. 458–467. doi:10.1007/978-981-13-2384-3_43.

[50] Z. Tong, J. Gao, A. Sha, L. Hu, S. Li, Convolutional neural network for asphalt pavement surface texture analysis, Computer-Aided Civil and Infrastructure Engineering 33 (12) (2018) 1056–1072. doi:10.1111/mice.12406.

[51] M. Lin, Q. Chen, S. Yan, Network in network, in: International Conference on Learning Representations (ICLR 2014), Banff, Canada, 2014, pp. 1–10.

[52] C. Lee, P. Gallagher, Z. Tu, Generalizing pooling functions in cnns: Mixed, gated, and tree, IEEE Transactions on Pattern Analysis and Machine Intelligence 40 (4) (2018) 863–875. doi:10.1109/TPAMI.2017.2703082.

[53] D. Mishkin, J. Matas, All you need is a good init (2015). arXiv:1511.06422.

[54] J. T. Springenberg, A. Dosovitskiy, T. Brox, M. Riedmiller, Striving for simplicity: The all convolutional net (2014). arXiv:1412.6806.

[55] H. Sak, A. Senior, F. Beaufays, Long short-term memory recurrent neural network architectures for large scale acoustic modeling, in: Fifteenth Annual Conference of the International Speech Communication Association, Singapore, 2014, pp. 338–342.

[56] X. Li, X. Wu, Constructing long short-term memory based deep recurrent neural networks for large vocabulary speech recognition, in: 2015 IEEE International Conference on Acoustics, Speech and Signal Processing (ICASSP), IEEE, Brisbane, QLD, Australia, 2015, pp. 4520–4524. doi:10.1109/ICASSP.2015.7178826.

[57] T. Mikolov, M. Karafiát, L. Burget, J. Černockỳ, S. Khudanpur, Recurrent neural network based language model, in: Eleventh annual conference of the international speech communication association, 2010.

[58] N. Pathak, D. Lachut, N. Roy, N. Banerjee, R. Robucci, Non-intrusive air leakage detection in residential homes, in: Proceedings of the 19th International Conference on Distributed Computing and Networking, ACM, New York, NY, USA, 2018, p. 31. doi:10.1145/3154273.3154345.

[59] A. Zhang, K. C. Wang, Y. Fei, Y. Liu, C. Chen, G. Yang, J. Q. Li, E. Yang, S. Qiu, Automated pixel-level pavement crack detection on 3D asphalt surfaces with a recurrent neural network, Computer-Aided Civil and Infrastructure Engineering 34 (3) (2019) 213–229. doi:10.1111/mice.12409.

[60] L. Mauch, B. Yang, A new approach for supervised power disaggregation by using a deep recurrent LSTM network, in: 2015 IEEE Global Conference on Signal and Information Processing (GlobalSIP), IEEE, Orlando, FL, USA, 2015, pp. 63–67. doi:10.1109/GlobalSIP.2015.7418157.

[61] P. P. M. do Nascimento, Applications of deep learning techniques on NILM, Diss. Universidade Federal do Rio de Janeiro.

[62] L. Theis, M. Bethge, Generative image modeling using spatial LSTMs, in: Advances in Neural Information Processing Systems, 2015, pp. 1927–1935.

[63] K. Gregor, I. Danihelka, A. Graves, D. J. Rezende, D. Wierstra, Draw: A recurrent neural network for image generation (2015). arXiv:1502.04623.

[64] F. Visin, K. Kastner, K. Cho, M. Matteucci, A. Courville, Y. Bengio, Renet: A recurrent neural network based alternative to convolutional networks (2015). arXiv:1505.00393.

[65] J. Chung, C. Gulcehre, K. Cho, Y. Bengio, Empirical evaluation of gated recurrent neural networks on sequence modeling (2014). arXiv:1412.3555.

[66] W. Byeon, T. M. Breuel, F. Raue, M. Liwicki, Scene labeling with LSTM recurrent neural networks, in: Proceedings of the IEEE Conference on Computer Vision and Pattern Recognition, Boston, MA, USA, 2015, pp. 3547–3555. doi:10.1109/CVPR.2015.7298977.

[67] Z. Yan, H. Zhang, Y. Jia, T. Breuel, Y. Yu, Combining the best of convolutional layers and recurrent layers: A hybrid network for semantic segmentation (2016). arXiv:1603.04871.

[68] S. Bell, C. Lawrence Zitnick, K. Bala, R. Girshick, Inside-outside net: Detecting objects in context with skip pooling and recurrent neural networks, in: The IEEE Conference on Computer Vision and Pattern Recognition (CVPR), Las Vegas, NV, USA, 2016, pp. 2874–2883. doi:10.1109/CVPR.2016.314.

[69] A. Graves, A.-r. Mohamed, G. Hinton, Speech recognition with deep recurrent neural networks, in: 2013 IEEE international conference on acoustics, speech and signal processing, IEEE, Vancouver, BC, Canada, 2013, pp. 6645–6649. doi:10.1109/ICASSP.2013.6638947.

[70] G. E. Hinton, R. R. Salakhutdinov, Reducing the dimensionality of data with neural networks, Science 313 (5786) (2006) 504–507. doi:10.1126/science.1127647.

[71] J. Li, M.-T. Luong, D. Jurafsky, A hierarchical neural autoencoder for paragraphs and documents (2015). arXiv:1506.01057.

[72] C.-Y. Huang, O. T.-C. Chen, G.-Z. Wu, C.-C. Chang, C.-L. Hu, Ultrasound imaging improved by the context encoder reconstruction generative adversarial network, in: 2018 IEEE International Ultrasonics Symposium (IUS), IEEE, Kobe, Japan, 2018, pp. 1–4. doi:10.1109/ULTSYM.2018.8579658.

[73] F. Picetti, G. Testa, F. Lombardi, P. Bestagini, M. Lualdi, S. Tubaro, Convolutional autoencoder for landmine detection on GPR scans, in: 2018 41st International Conference on Telecommunications and Signal Processing (TSP), IEEE, Athens, Greece, 2018, pp. 1–4. doi:10.1109/TSP.2018.8441206.

[74] Z. Tong, J. Gao, Z. Wang, Y. Wei, H. Dou, A new method for CF morphology distribution evaluation and CFRC property prediction using cascade deep learning, Construction and Building Materials 222 (2019) 829–838. doi:10.1016/j.conbuildmat.2019.06.160.

[75] Z. Tong, H. Guo, J. Gao, Z. Wang, A novel method for multi-scale carbon fiber distribution characterization in cement-based composites, Construction and Building Materials 218 (2019) 40–52. doi:10.1016/j.conbuildmat.2019.05.115.

[76] Y.-l. Boureau, Y. L. Cun, et al., Sparse feature learning for deep belief networks, in: Advances in Neural Information Processing Systems, 2008, pp. 1185–1192.

[77] P. Vincent, H. Larochelle, I. Lajoie, Y. Bengio, P.-A. Manzagol, Stacked denoising autoencoders: Learning useful representations in a deep network with a local denoising criterion, Journal of Machine Learning Research 11 (Dec) (2010) 3371–3408.

[78] S. Rifai, P. Vincent, X. Muller, X. Glorot, Y. Bengio, Contractive auto-encoders: Explicit invariance during feature extraction, in: Proceedings of the 28th International Conference on International Conference on Machine Learning, Omnipress, Bellevue, Washington, USA, 2011, pp. 833–840.

[79] G. E. Hinton, S. Osindero, Y.-W. Teh, A fast learning algorithm for deep belief nets, Neural Computation 18 (7) (2006) 1527–1554. doi:10.1162/neco.2006.18.7.1527.

[80] A. Ioannidou, E. Chatzilari, S. Nikolopoulos, I. Kompatsiaris, Deep learning advances in computer vision with 3D data: A survey, ACM Computing Surveys (CSUR) 50 (2) (2017) 20. doi:10.1145/3042064.

[81] J. Becker, T. C. Havens, A. Pinar, T. J. Schulz, Deep belief networks for false alarm rejection in forward-looking ground-penetrating radar, in: Detection and Sensing of Mines, Explosive Objects, and Obscured Targets

XX, Vol. 9454, International Society for Optics and Photonics, 2015, p. 94540W. doi:10.1117/12.2176855.

[82] T. C. Havens, D. T. Anderson, K. Stone, J. Becker, A. J. Pinar, Computational intelligence methods in forward-looking explosive hazard detection, in: Recent Advances in Computational Intelligence in Defense and Security, Springer, Cham,Germany, 2016, pp. 13–44. doi:10.1007/978-3-319-26450-9_2.

[83] G. E. Hinton, N. Srivastava, A. Krizhevsky, I. Sutskever, R. R. Salakhutdinov, Improving neural networks by preventing co-adaptation of feature detectors (2012). arXiv:1207.0580.

[84] G. Hinton, O. Vinyals, J. Dean, Distilling the knowledge in a neural network (2015). arXiv:1503.02531.

[85] Y. Bengio, P. Lamblin, D. Popovici, H. Larochelle, Greedy layer-wise training of deep networks, in: Advances in neural information processing systems, MITP, 2007, pp. 153–160.

[86] Y.-y. He, B.-q. Li, Y.-s. Guo, T.-n. Wang, Y. Zhu, An interpretation model of GPR point data in tunnel geological prediction, in: Eighth International Conference on Graphic and Image Processing (ICGIP 2016), Vol. 10225, International Society for Optics and Photonics, SPIE, 2017, p. 102252J. doi:10.1117/12.2266226.

[87] W. Wang, Human detection based on radar sensor network in natural disaster, in: Geological Disaster Monitoring Based on Sensor Networks, Springer, Singapore, 2019, pp. 109–134. doi:10.1007/978-981-13-0992-2_8.

[88] Z. Tong, D. Yuan, J. Gao, Y. Wei, H. Dou, Pavement-distress detection using ground-penetrating radar and network in networks, Construction and Building Materials 233 (2020) 117352. doi:10.1016/j.conbuildmat.2019.117352.

[89] I. Giannakis, A. Giannopoulos, C. Warren, A machine learning-based fast-forward solver for ground penetrating radar with application to full-waveform inversion, IEEE Transactions on Geoscience and Remote Sensingdoi:10.1109/tgrs.2019.2891206.

[90] Y. Jia, E. Shelhamer, J. Donahue, S. Karayev, J. Long, R. Girshick, S. Guadarrama, T. Darrell, Caffe: Convolutional architecture for fast feature embedding, in: Proceedings of the 22Nd ACM International Conference on Multimedia, MM '14, ACM, New York, NY, USA, 2014, pp. 675–678. doi:10.1145/2647868.2654889.

[91] M. Abadi, P. Barham, J. Chen, Z. Chen, A. Davis, J. Dean, M. Devin, S. Ghemawat, G. Irving, M. Isard, et al., Tensorflow: A system for large-scale machine learning, in: 12th USENIX Symposium on Operating Systems Design and Implementation (OSDI 16), USENIX Association, 2016, pp. 265–283.

[92] Z. Xiang, A. Rashidi, G. G. Ou, Robotics, automation, and control, Computing in Civil Engineering 2019doi:10.1061/9780784482438.054.

[93] U. Ozkaya, L. Seyfi, Deep dictionary learning application in GPR B-scan images, Signal, Image and Video Processing 12 (8) (2018) 1567–1575. doi:10.1007/s11760-018-1313-x.

[94] S. Lameri, F. Lombardi, P. Bestagini, M. Lualdi, S. Tubaro, Landmine detection from GPR data using convolutional neural networks, in: 2017 25th European Signal Processing Conference (EUSIPCO), IEEE, Kos, Greece, 2017, pp. 508–512. doi:10.23919/EUSIPCO.2017.8081259.

[95] K. Ishitsuka, S. Iso, K. Onishi, T. Matsuoka, Object detection in ground-penetrating radar images using a deep convolutional neural network and image set preparation by migration, International Journal of Geophysics 2018 (2018) 9365184. doi:10.1155/2018/9365184.

[96] K. Dinh, N. Gucunski, T. H. Duong, An algorithm for automatic localization and detection of rebars from GPR data of concrete bridge decks, Automation in Construction 89 (2018) 292–298. doi:10.1016/j.autcon.2018.02.017.

[97] L. E. Besaw, P. J. Stimac, Deep convolutional neural networks for classifying GPR B-scans, in: Detection and Sensing of Mines, Explosive Objects, and Obscured Targets XX, Vol. 9454, International Society for Optics and Photonics, SPIE, 2015, p. 945413. doi:10.1117/12.2176250.

[98] S. Ren, K. He, R. Girshick, J. Sun, Faster r-cnn: Towards real-time object detection with region proposal networks, in: Advances in neural information processing systems, 2015, pp. 91–99.

[99] W. Lei, F. Hou, J. Xi, Q. Tan, M. Xu, X. Jiang, G. Liu, Q. Gu, Automatic hyperbola detection and fitting in GPR B-scan image, Automation in Construction 106 (2019) 102839. doi:10.1016/j.autcon.2019.102839.

[100] X. Xu, Y. Lei, F. Yang, Railway subgrade defect automatic recognition method based on improved Faster R-CNN, Scientific Programming 2018 (2018) 4832972. doi:10.1155/2018/4832972.

[101] P. F. Felzenszwalb, R. B. Girshick, D. McAllester, D. Ramanan, Object detection with discriminatively trained part-based models, IEEE Transactions on Pattern Analysis and Machine Intelligence 32 (9) (2009) 1627–1645. doi:10.1109/TPAMI.2009.167.

[102] M.-T. Pham, S. Lefèvre, Buried object detection from B-scan ground penetrating radar data using Faster-RCNN, in: IGARSS 2018-2018 IEEE International Geoscience and Remote Sensing Symposium, IEEE, Valencia, Spain, 2018, pp. 6804–6807. doi:0.1109/IGARSS.2018.8517683.

[103] R. Shwartz-Ziv, N. Tishby, Opening the black box of deep neural networks via information, CoRR abs/1703.00810. arXiv:1703.00810.
URL http://arxiv.org/abs/1703.00810

[104] J. K. Alvarez, S. Kodagoda, Application of deep learning image-to-image transformation networks to GPR radargrams for sub-surface imaging in infrastructure monitoring, in: 2018 13th IEEE Conference on Industrial Electronics and Applications (ICIEA), IEEE, Wuhan, China, 2018, pp. 611–616. doi:10.1109/ICIEA.2018.8397788.

[105] Z. Wang, A. C. Bovik, H. R. Sheikh, E. P. Simoncelli, et al., Image quality assessment: from error visibility to structural similarity, IEEE Transactions on Image Processing 13 (4) (2004) 600–612. doi:10.1109/TIP.2003.819861.

[106] N. Kim, S. Kim, Y.-K. An, J.-J. Lee, A novel 3d GPR image arrangement for deep learning-based underground object classification, International Journal of Pavement Engineering (2019) 1–12doi:10.1080/10298436.2019.1645846.

[107] J. Gao, D. Yuan, Z. Tong, J. Yang, D. Yu, Autonomous pavement distress detection using ground penetrating radar and region-based deep learning, Measurement 164 (2020) 108077. doi:https://doi.org/10.1016/j.measurement.2020.108077.

[108] P. Rodriguez, G. Cucurull, J. Gonzàlez, J. M. Gonfaus, K. Nasrollahi, T. B. Moeslund, F. X. Roca, Deep pain: Exploiting long short-term memory networks for facial expression classification, IEEE transactions on cybernetics.

[109] A. Krizhevsky, G. Hinton, et al., Learning multiple layers of features from tiny images, Tech. rep., Citeseer, University of Toronto, Toronto. (2009).

[110] J. Deng, W. Dong, R. Socher, L. Li, Kai Li, Li Fei-Fei, ImageNet: A large-scale hierarchical image database, in: 2009 IEEE Conference on Computer Vision and Pattern Recognition, Miami, FL, USA, 2009, pp. 248–255. doi:10.1109/CVPR.2009.5206848.

[111] M. Defferrard, K. Benzi, P. Vandergheynst, X. Bresson, Fma: A dataset for music analysis (2016). arXiv:1612.01840.

[112] J. Bralich, D. Reichman, L. M. Collins, J. M. Malof, Improving convolutional neural networks for buried target detection in ground penetrating radar using transfer learning via pretraining, in: Detection and Sensing of Mines, Explosive Objects, and Obscured Targets XXII, Vol. 10182, International Society for Optics and Photonics, SPIE, 2017, pp. 198 – 208. doi:10.1117/12.2263112.

[113] D. Reichman, L. M. Collins, J. M. Malof, Some good practices for applying convolutional neural networks to buried threat detection in ground penetrating radar, in: 2017 9th International Workshop on Advanced Ground Penetrating Radar (IWAGPR), IEEE, Edinburgh, UK, 2017, pp. 1–5. doi:10.1109/IWAGPR.2017.7996100.

[114] E. Aydin, S. E. Y. Erdem, Transfer and multitask learning using convolutional neural networks for buried wire detection from ground penetrating radar data, in: Detection and Sensing of Mines, Explosive Objects, and Obscured Targets XXIV, Vol. 11012, International Society for Optics and Photonics, SPIE, Maryland, United States, 2019, pp. 259 – 270. doi:10.1117/12.2518875.

[115] O. Russakovsky, J. Deng, H. Su, J. Krause, S. Satheesh, S. Ma, Z. Huang, A. Karpathy, A. Khosla, M. Bernstein, et al., Imagenet large scale visual recognition challenge, International Journal of Computer Vision 115 (3) (2015) 211–252. doi:10.1007/s11263-015-0816-y.

[116] R. Shwartz-Ziv, N. Tishby, Opening the black box of deep neural networks via information (2017). arXiv:1703.00810.

[117] J. M. Malof, J. Bralich III, D. Reichman, L. M. Collins, Improving the histogram of oriented gradient feature for threat detection in ground penetrating radar by implementing it as a trainable convolutional neural network, in: Detection and Sensing of Mines, Explosive Objects,

and Obscured Targets XXIII, Vol. 10628, International Society for Optics and Photonics, Florida, United States, 2018, p. 106280D. doi:10.1117/12.2305797.

[118] J. Sonoda, T. Kimoto, Object identification form GPR images by deep learning, in: 2018 Asia-Pacific Microwave Conference (APMC), IEEE, Kyoto, Japan, 2018, pp. 1298–1300. doi:10.23919/APMC.2018.8617556.

[119] C. Veal, J. Dowdy, B. Brockner, D. T. Anderson, J. E. Ball, G. Scott, Generative adversarial networks for ground penetrating radar in hand held explosive hazard detection, in: Detection and Sensing of Mines, Explosive Objects, and Obscured Targets XXIII, Vol. 10628, International Society for Optics and Photonics, Florida, United States, 2018, p. 106280T. doi:10.1117/12.2307261.

[120] L. Perez, J. Wang, The effectiveness of data augmentation in image classification using deep learning (2017). arXiv:1712.04621.

[121] V. Vovk, A. Gammerman, G. Shafer, Algorithmic learning in a random world, Springer Science & Business Media, 2005. doi:10.1007/b106715.

[122] R. Sakaguchi, M. Crosskey, D. Chen, B. Walenz, K. Morton Jr, Convolutional neural network based sensor fusion for forward looking ground penetrating radar, in: Detection and Sensing of Mines, Explosive Objects, and Obscured Targets XXI, Vol. 9823, International Society for Optics and Photonics, Maryland, United States, 2016, p. 98231J. doi:10.1117/12.2224125.

[123] T. Denœux, Logistic regression, neural networks and Dempster-Shafer theory: A new perspective, Knowledge-Based Systems 176 (2019) 54–67. doi:10.1016/j.knosys.2019.03.030.

[124] Z. Liu, Q. Pan, J. Dezert, J.-W. Han, Y. He, Classifier fusion with contextual reliability evaluation, IEEE Transactions on Cybernetics 48 (5) (2017) 1605–1618. doi:10.1109/TCYB.2017.2710205.

[125] Y. Hechtlinger, B. PÃşczos, L. Wasserman, Cautious deep learning (2018). arXiv:1805.09460.

[126] Z. Tong, P. Xu, T. Denœux, ConvNet and Dempster-Shafer Theory for Object Recognition, in: Scalable Uncertainty Management, Springer International Publishing, Compiègne, France, 2019, pp. 368–381. doi:10.1007/978-3-030-35514-2_27.

[127] T. Denœux, Analysis of evidence-theoretic decision rules for pattern classification, Pattern Recognition 30 (7) (1997) 1095–1107. doi:10.1016/S0031-3203(96)00137-9.

[128] L. Ma, T. Denœux, Making set-valued predictions in evidential classification: A comparison of different approaches, in: the Eleventh International Symposium on Imprecise Probabilities: Theories and Applications, Thagaste, Ghent, Belgium, 2019, pp. 276–285.

[129] T. Denoeux, A neural network classifier based on Dempster-Shafer theory, IEEE Transactions on Systems, Man, and Cybernetics-Part A: Systems and Humans 30 (2) (2000) 131–150. doi:10.1109/3468.833094.